Journal of Bio- and Tribo-Corrosion (2023) 9:33
https://doi.org/10.1007/s40735-023-00751-y

Corrosion Inhibiting by Some Organic Heterocyclic Inhibitors Through Langmuir Adsorption Mechanism on the Al-*X* (*X* = Mg/Ga/Si) Alloy Surface: A Study of Quantum Three-Layer Method of CAM-DFT/ONIOM

Fatemeh Mollaamin[1] · **Majid Monajjemi**[2]

Received: 17 November 2022 / Revised: 19 February 2023 / Accepted: 14 March 2023 / Published online: 31 March 2023

Abstract
The physicochemical attributes of inhibitor → metal & metal alloys nanosheet can be one of the fundamental factors for recognizing determining and selecting the Langmuir adsorption through IR, NMR, NQR, NBO, UV–VIS, HOMO/LUMO, and charge distribution and other quantum attributes. Then, the fluctuation of occupancy of natural bond orbitals has been estimated for pyridine → Al–Al, pyridine → Al–Mg, pyridine → Al–Ga, pyridine → Al–Si; 2-picoline → Al–Al, 2-picoline → Al–Mg, 2-picoline → Al–Ga, 2-picoline → Al–Si; 3-picoline → Al–Al, 3-picoline → Al–Mg, 3-picoline → Al–Ga, 3-picoline → Al–Si, 4-picoline → Al–Al, 4-picoline → Al–Mg, 4-picoline → Al–Ga, 4-picoline → Al–Si, and 2,4-lutidine → Al–Al, 2,4-lutidine → Al–Mg, 2,4-lutidine → Al–Ga, and 2,4-lutidine → Al–Si through the Langmuir adsorption process due to concerning the nitrogen atom in the benzene ring of related heterocyclic compounds becoming close to the monolayer nanosurface of aluminum and its alloys. Nuclear magnetic resonance has certainly has focused on the aluminum shielding in the intra-atomic interaction with magnesium, gallium, and silicon and simultaneously interatomic interaction with nitrogen atoms in organic heterocyclic inhibitors through variety of high, medium, and low layers of ONIOM method. In addition, on the basis of the computed amounts of UV–VIS spectra for pyridine and its family adsorbing on the Al alloy surface, there are maximum adsorption bands between 150 and 240 nm. Two maximum adsorption bands for pyridine, 2-picoline, 3-picoline, and 4-picoline are at 200 nm and 250 nm. Besides, it has been observed two maximum adsorption bands for 2,4-lutidine around 170 nm and 210 nm, respectively.

Keywords Langmuir adsorption · Organic heterocyclic inhibitors · Al–Mg · Al–Ga · Al–Si · ONIOM · CAM-B3LYP/EPR-III, LANL2DZ, 6–31 + G(d,p) · NMR · NQR · NBO · IR · UV–VIS · HOMO · LUMO

1 Introduction

Material choice is one of the common methodologies applied to avoid corrosion. Apart from specific necessities linked to the actual usage and the corrosion ambiance, there are also common parameters to be remarked in material choice. The mechanical and physical characteristics including strength, hardness, flexibility, and density, stability to corrosion, and to service situations are among the most important [1–4].

In some researches, an ionic structure has been explored containing several organic and inorganic anions and organic cations in liquid state with close to room temperature [5–8]. It has the benefits of non-fugacious, extended electrochemical frame, vast liquid temperature limitation, appropriate thermal resistance, conductivity and changing mixture of characteristics, and is extendedly employed in the variety of scientific and technological branches [9–16]. It is clear that heterocyclic structures consisting of N atoms are effective corrosion inhibitors for disparate groups of metals in diverse acidic media [17–27].

Because diverse characteristics of organic structures are to be represented, it is essential that the electrons of a set of organic structures be discussed. Therefore, operated organic compounds as corrosion stoppers were chosen and

✉ Fatemeh Mollaamin
smollaamin@gmail.com

[1] Department of Biomedical Engineering, Faculty of Engineering and Architecture, Kastamonu University, Kastamonu, Turkey

[2] Department of Chemical Engineering, Central Tehran Branch, Islamic Azad University, Tehran, Iran

determined based on their physical and chemical characteristics [28, 29], and little consideration has been dedicated to the quantitative estimation of the internal and steric influence of these compounds upon their inhibition yield. In other works, it has been studied by the interaction between imidazole and the aluminum surface which is often employed in experimental researches [30–45].

It has been studied that pyridine family compounds have been broadly applied through their intense polarity and increasing potency in ionic liquids and solution. It is seen that some compounds including nicotine amide, pyridine-2-formamide, and pyridine-4-formamide can be employed as efficient increasing factors for electro-deposition of aluminum in [Bmim] $Cl/AlCl_3$ with the unclear mechanism in finding the intermolecular interaction between additives and electrode, charge distribution, and adsorption comportment [46–57].

The present work intends to accomplish an extension of the previous investigations [58–60] of the role of pyridine and its family compounds as corrosion inhibitor for aluminum and its alloys containing Al–Al, Al–Mg, Al–Ga, and Al–Si nanosheets through CAM-B3LYP/EPR-III, LANL2DZ,6–31 + G(d,p) theoretical methods using NMR, IR, NQR, NBO, ESP, and UV–VIS spectroscopy and HOMO–LUMO orbital frontier analysis.

2 Modeling Strategy and Computational Method

Aluminum (Al) has high thermal and electrical conductivity with acceptable flexibility reflectivity and a low weight [61–63]. However, the special alloying elements are Cu, Mg, Mn, Si, Sn, Ni, and Zn. Light weight and corrosion resistance of aluminum alloys make them suitable in engineering structures and components [61, 64–83].

The aim of this paper is the application of nitrogen heterocyclic compounds as corrosion inhibitors for aluminum nanosheet and its alloy surfaces (Scheme 1a–d).

The spectroscopy of IR for each of these compounds in Scheme 1 was observed in the maximum frequency approximately between 1000 and 1700 cm^{-1},Al–Al; 1000 and 1800 cm^{-1}, Al–Mg; 1000 and 1600 cm^{-1}, Al–Ga; and 1400 and 2400 cm^{-1}, Al–Si, respectively, concerning the strongest peaks about 1500 cm^{-1}, Al–Al; 1000 cm^{-1} and 1800 cm^{-1}, Al–Mg; 1400 cm^{-1}, 1500 cm^{-1}, and 1600 cm^{-1}, Al–Ga; 1500 cm^{-1} and 2100 cm^{-1}, Al–Si, respectively (Scheme 1a–d).

For improving the quantum mechanics and molecular mechanic "QM/MM" electrostatic interactions and containing polarization of the "QM" wave function by the "MM" environment, the one-electron term defining the atomic charges in the MM environment system might increase to the QM Hamiltonian that is employed to the QM approach [84, 85].

$$E_{QM/MM} = E_{QM} + E_{MM} + E_{QM-MM}. \tag{1}$$

In theoretical "ONIOM" method, any combination of three levels in the reducing order of accuracy can be accepted in ONIOM3. The typically acceptable levels are high (QM1), medium (QM2), and low (QM3or MM), where high level (QM1) often is an ab initio or DFT method, medium level (QM2) is a low-level ab initio, DFT, or semi-empirical (SE) QM method, and low level is an SE QM method or an MM method (Scheme 2) [86].

So, the mixing of three levels of QM1, QM2, and QM3 in reducing order of accuracy has been assigned containing high, medium, and low levels of theory [87].

$$E_{\mathrm{ONIOM}} = E_{\mathrm{high(QM1)}} + E_{\mathrm{medium(QM2)}} + E_{\mathrm{low(QM3)}}. \tag{2}$$

The "ONIOM" method could be lightly extended and popularized to an n-layer method [88, 89]:

$$E_{\mathrm{ONIOM}n} = \sum_{i=1}^{n} E[\mathrm{level}(i), model(n+1-i)] - \sum_{i=2}^{n} E[\mathrm{level}(i), model(n+2-i)]. \tag{3}$$

This three-layered form has been employed to activate barriers for the pyridine, 2-picoline, 3-picoline, 4-picoline and 2,4-lutidine onto monolayer Al-X (X = Al, Mg, Ga, Si) surface toward forming the Langmuir adsorption complexes ,including pyridine → Al–Al, pyridine → Al–Mg, pyridine → Al–Ga, pyridine → Al–Si; 2-picoline → Al–Al, 2-picoline → Al–Mg, 2-picoline → Al–Ga, 2-picoline → Al–Si; 3-picoline → Al–Al, 3-picoline → Al–Mg, 3-picoline → Al–Ga, 3-picoline → Al–Si, 4-picoline → Al–Al, 4-picoline → Al–Mg, 4-picoline → Al–Ga, 4-picoline → Al–Si, and 2,4-lutidine → Al–Al, 2,4-lutidine → Al–Mg, 2,4- lutidine → Al–Ga, and 2,4- lutidine → Al–Si (Schemes 1 and 2).

Density functional theory (DFT) calculations have been performed using Gaussian 16 revision C.01 [90–104] software. The calculation have been carried out using LANL2DZ, EPR-III, 6 – 31 + G(d,p) basis sets to determine chemical shielding, frequencies, occupancy and hybrid of natural atomic orbitals, electrostatic potential, electronic potential, energy gap of frontier orbitals, natural atomic charges, electron density mapping, and other quantum

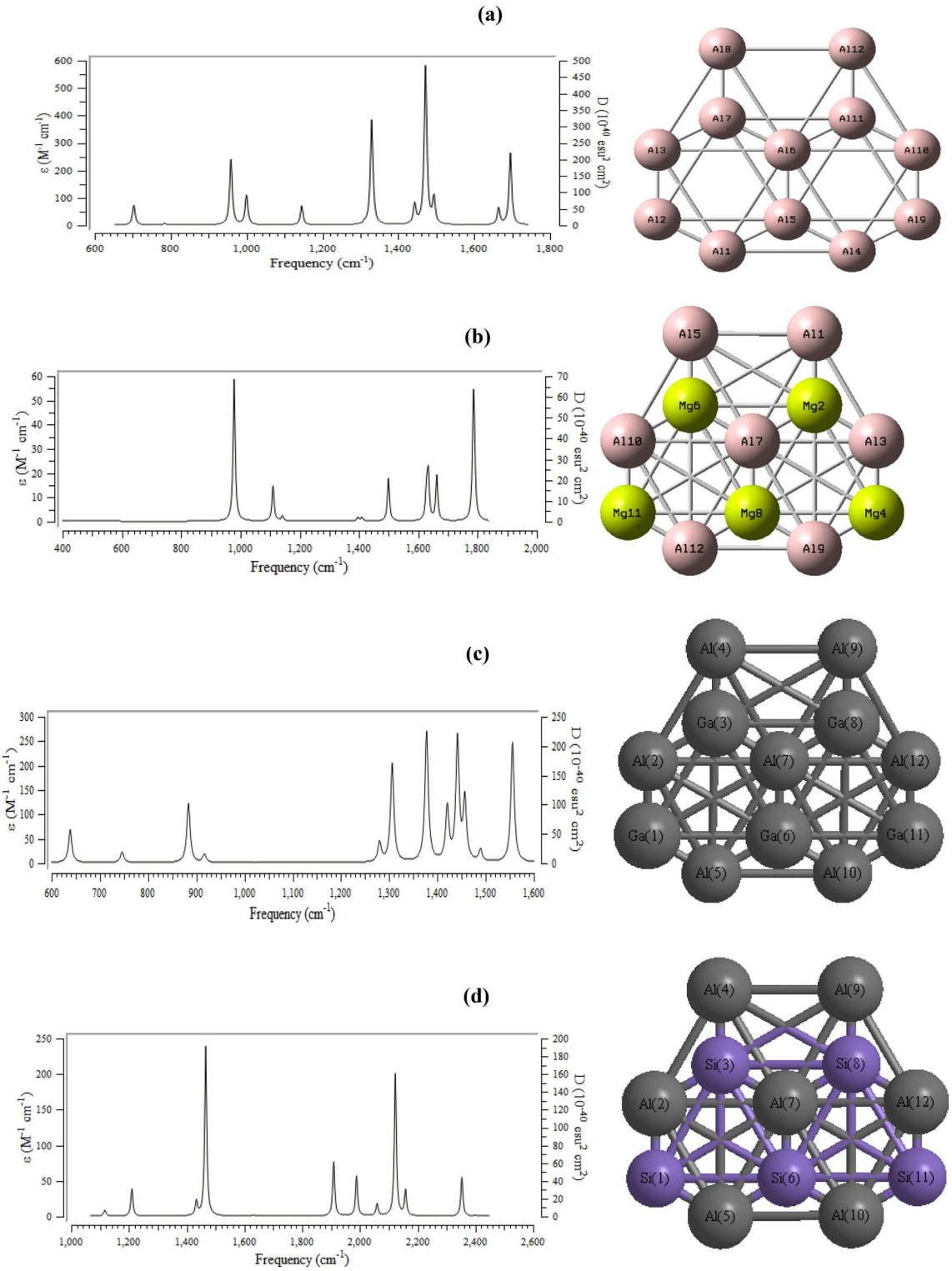

Scheme 1 IR spectra for aluminum alloys (Al-*X*) consisting of **a** Al–Al, **b** Al–Mg, **c** Al–Ga, and **d** Al–Si

properties for this investigation. The rigid PES has been run at CAM-B3LYP/EPR-III, LANL2DZ,6 − 31 + G(d,p) for pyridine and its family (2-picoline, 3-picoline, 4-picoline, and 2,4-lutidine) adsorbed onto aluminum and its alloys in which the small energy difference between the formations of nitrogen → aluminum complexes can

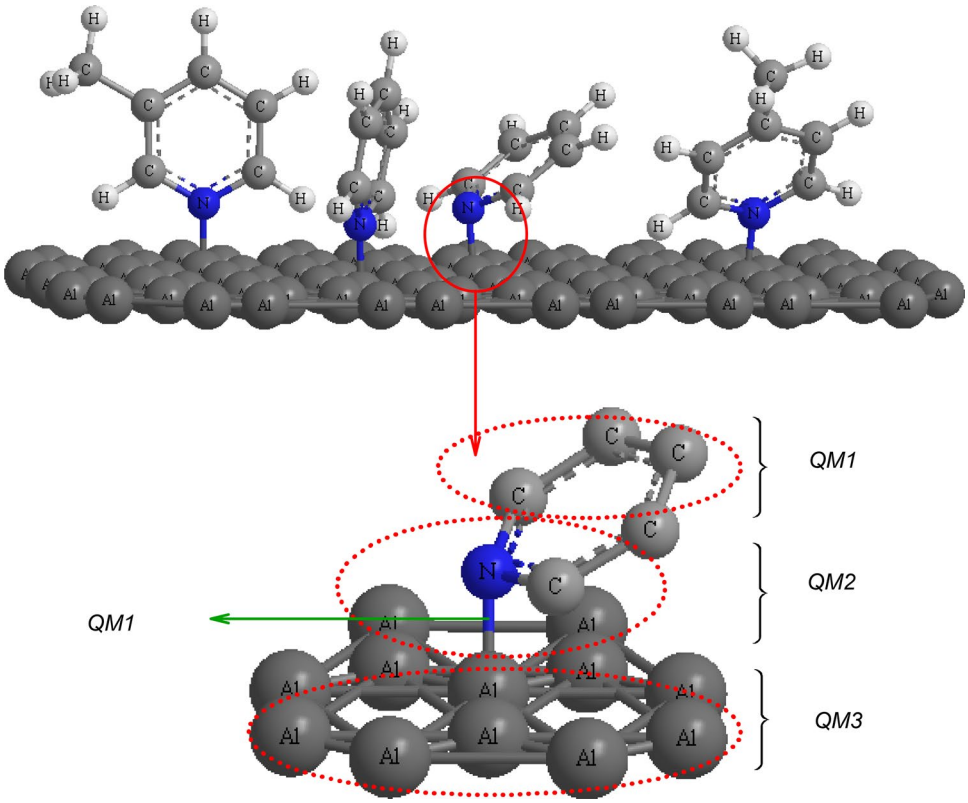

Scheme 2 Process of physical and chemical adsorption of pyridine and its family (2-picolone, 3-picoline, 4-picoline and 2,4-lutidine onto Aluminum surface in different levels containing high, medium, and low levels by theoretical ONIOM method of calculation

lead us to an appropriate coated surface for ignoring the corrosion.

3 Results and Discussion

3.1 Nuclear Magnetic Resonance

NMR data of isotropic (σ_{iso}), anisotropic shielding tensor (σ_{aniso}), and eigenvalues of chemical shielding including σ_{11}, σ_{22}, and σ_{33} for pyridine → Al–Al, 2-picoline → Al–Al, 3-picoline → Al–Al, 4-picoline → Al–Al, and 2,4-lutidine → Al–Al have been calculated using Gaussian 16 revision C.01 program software [103] and reported in Table 1.

The calculation of nuclear magnetic resonance "NMR" for chemical shifts for assigning the structural and geometrical of compounds has been accomplished. In fact, Gauge Invariant Atomic Orbital "GIAO" method has been suggested as an accurate method for "NMR" parameter calculations, and "ONIOM" has obtained much attention for achieving "NMR" chemical shifts in inhibitor-surface complexes, for instance, isotropic chemical shielding becomes [67, 105, 106]

$$\sigma_{iso,ONIOM} = \sigma_{iso,high(QM1)} + \sigma_{iso,medium(QM2)} + \sigma_{iso,low(QM3)}. \quad (4)$$

In Fig. 1, it was that the isotropic and anisotropy shielding augment with the occupancy and consequently the negative charge of nitrogen atom in pyridine and its derivatives diffusing onto Al–Al surface. It was illustrated that the curve of "N" atom has the same attitude but a remarkable deviation from "C" and "H" atoms (Fig. 1a–e).

The heterocyclic organic inhibitors of pyridine, 2-picoline, 3-picoline, a 4-picoline, and 2,4-lutidine have approximately shown the identical behavior (20–80 ppm) (Fig. 1a–e). The sharpest peak of NMR spectrum has been almost observed in 25 ppm for these compounds. The weakest peaks of NMR spectrum have approximately appeared in 80 ppm for all five heterocyclic organic inhibitors containing pyridine, 2-picoline, 3-picoline, 4-picoline, and 2,4-lutidine (Fig. 1a–e). Moreover, in Fig. 1a–e, it has been shown that an electrostatic potential (ESP) surface or map of a molecule which presents the partial distribution of change along the molecule's surface helps to assign molecular polarity.

Moreover, the complexes of Langmuir adsorption consisting of pyridine → Al–Ga, 2-picoline → Al–Mg, 3-picoline → Al–Ga, 4-picoline → Al–Si, and 2,4-lutidine → Al–Al have exhibited maximum band wavelengths approximately between 10 and 2500 ppm for these compounds (Fig. 1a′–e′). In fact, the sharpest peaks for pyridine → Al–Ga,10–500 ppm; 2-picoline → Al–Mg, 10–200 ppm; 3-picoline → Al–Ga, 10 ppm and 2400 ppm;

Table 1 NMR attributes of some atoms for pyridine →Al-Al, 2-picoline→Al-Al, 3-picoline→Al-Al,4-picoline →Al-Al, and 2,4- lutidine →Al-Al complexes in ppm

Pyridine→Al–Al										
ppm	N1	C2	C3	C4	C5	C6	H7	H8	H9	H10
σ_{11}	−415.85	−55.64	−55.63	−26.66	−34.22	−26.67	21.09	21.09	23.10	22.61
σ_{22}	−139.97	42.91	42.91	69.92	43.59	69.91	22.722	22.72	24.84	25.26
σ_{33}	298.57	158.46	158.47	183.69	189.46	183.68	27.39	27.39	27.93	27.67
σ_{iso}	−85.75	48.58	48.58	75.65	66.28	75.64	23.34	23.73	25.29	25.18
σ_{aniso}	576.48	164.83	164.83	162.05	184.78	162.06	5.48	5.48	3.96	3.73
2-picoline→Al–Al										
ppm	N1	C2	C3	C4	C7	H8	H9	H12	H13	H14
σ11	−427.99	−55.83	−55.26	-24.02	146.70	21.48	22.89	26.40	26.42	26.40
σ22	−124.18	50.05	21.75	73.55	165.11	22.72	24.28	28.80	30.97	28.80
σ33	296.99	157.68	156.07	173.92	193.64	27.42	29.99	35.05	35.04	35.05
σiso	−85.06	50.63	40.85	74.48	168.48	23.87	25.72	30.08	30.81	30.08
σaniso	573.08	160.57	172.82	149.16	37.74	5.32	6.40	7.45	6.34	7.45
3-picoline→Al–Al										
ppm	N1	C2	C3	C4	C7	H8	H9	H12	H13	H14
σ11	−460.67	−50.34	−53.59	−30.34	153.06	21.5865	21.09	25.97	26.71	25.97
σ22	−131.96	51.44	55.15	34.00	170.57	22.6655	21.40	29.16	30.89	29.16
σ33	305.98	160.37	150.63	186.06	195.53	27.6310	28.98	35.63	35.82	35.63
σiso	−95.55	53.82	50.73	63.24	173.05	23.9610	23.82	30.25	31.14	30.26
σaniso	602.29	159.82	149.84	184.22	33.72	5.5050	7.73	8.06	7.02	8.06
4-picoline→Al–Al										
ppm	N1	C2	C3	C5	C7	H8	H9	H12	H13	H14
σ11	−442.84	−54.86	−54.51	−37.56	150.36	21.56	21.43	25.92	26.38	25.92
σ22	−124.10	49.22	49.95	16.72	168.16	22.30	22.31	29.26	30.75	29.26
σ33	310.20	157.20	157.78	187.29	196.12	27.92	27.91	35.72	35.88	35.72
σiso	−85.58	50.52	51.07	55.48	171.55	23.93	23.88	30.30	31.00	30.30
σaniso	593.67	160.02	160.06	197.71	36.86	5.98	6.03	8.12	7.31	8.12
2, 4-lutidine→Al–Al										
ppm	N1	C2	C3	C5	C7	C8	H12	H13	H15	H16
σ11	−411.58	−54.35	−53.50	−37.39	146.94	150.72	26.42	26.27	25.87	26.35
σ22	−117.03	50.13	22.78	16.24	165.26	168.11	28.72	31.32	29.46	30.71
σ33	299.05	154.74	153.81	184.35	193.82	196.31	35.23	34.95	35.73	36.07
σiso	−76.52	50.17	41.03	54.40	168.67	171.72	30.13	30.85	30.35	31.04
σaniso	563.36	156.85	169.17	194.92	37.72	36.89	7.65	6.15	8.06	7.54

4-picoline → Al–Si, 10 ppm–200 ppm; and also 2,4-lutidine → Al–Al, 10 ppm–200 ppm, respectively (Fig. 1a′–e′).

3.2 Nuclear Quadrupole Resonance (NQR)

In this article, the calculated nuclear quadrupole resonance (NQR) frequency for pyridine and its heterocyclic derivatives is proportional to the product of the nuclear quadrupole moment, a property of the nucleus, and the "EFG" in the neighborhood of the nucleus [107–110].

In this work, the electric potential as the amount of work energy through transferring the electric charge from one site to another site in presence of electric field has been measured for pyridine, 2-picolone, 3-picoline, 4-picoline, and 2,4-lutidine adsorbing onto aluminum surface using

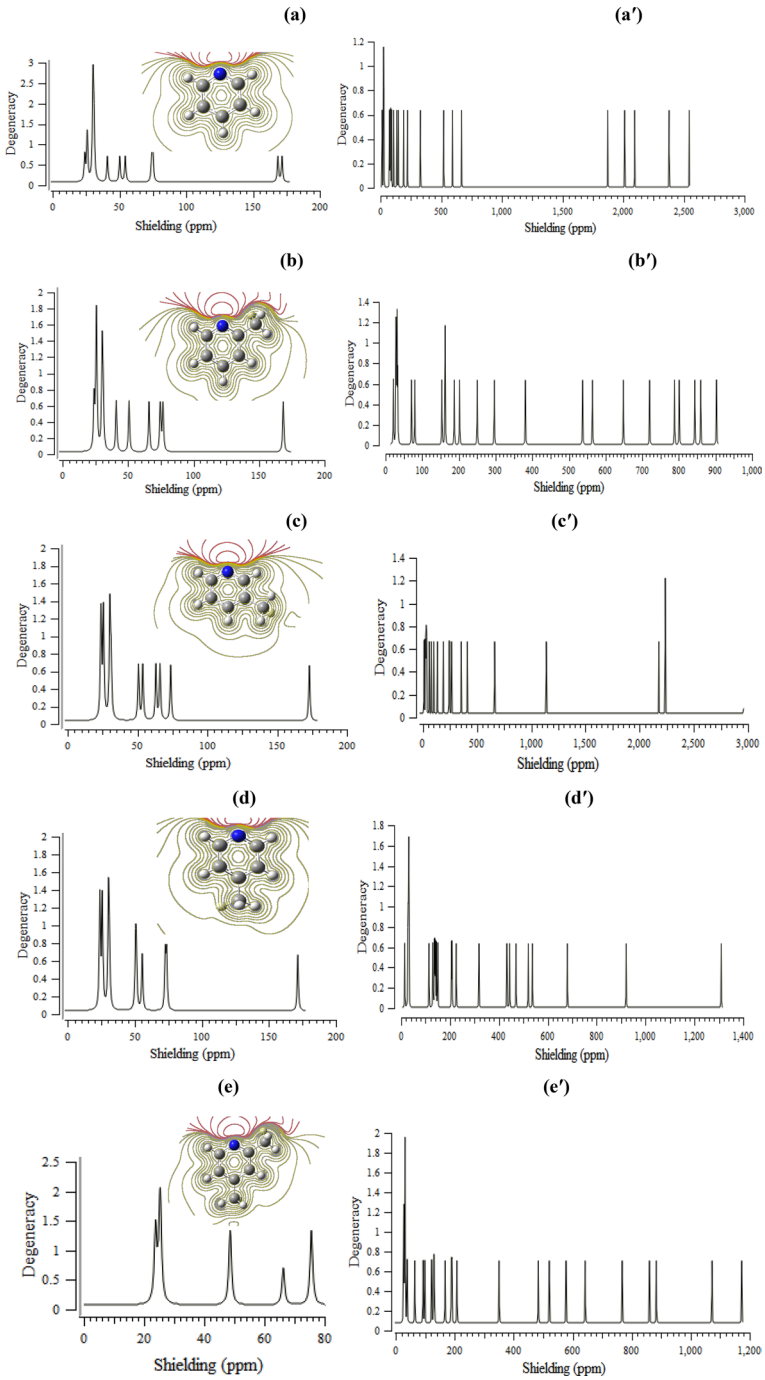

Fig. 1 Chemical shift of NMR spectroscopy for **a** pyridine and **a′** pyridine → Al–Ga; **b** 2-picoline and **b′** 2-picoline → Al–Mg; **c** 3-picoline and **c′** 3-picoline → Al–Ga; **d** 4-picoline and **d′** 4-picoline → Al–Si; and **e** 2,4-lutidine and **e′** 2,4-lutidine → Al–Al through the Langmuir adsorption mechanism by denoting the active N atom in heterocyclic compounds becoming near the nanosheet

CAM-B3LYP/EPR-III, LANL2DZ,6−31 + G(d,p) level of theory (Table 2).

Since the electric potential for a group of point charges is identical to the sum of the point charges of individual potentials, the measurements are done simply based on summation of potential fields which is scalar instead of summation of the electric fields.

In addition, in Fig. 2a–e, it has been plotted the electric potential of NQR method for elements of pyridine and its privatives that were adsorbed on the Al–Al surface using CAM-B3LYP/EPR-III, LANL2DZ,6−31 + G(d,p) theoretical level.

In Fig. 2a–d, the polynomial graphs (order = 2) of electric potential versus atomic charges of atoms for pyridine, 2-picoline, 3-picoline, 4-picoline, and 2,4-lutidine adsorbing on the Al–Al surface using CAM-B3LYP/EPR-III, LANL2DZ,6−31 + G(d,p) with relation coefficient of $R^2_{\text{pyridine}} = 0.7594$, $R^2_{\text{2-picoline}} = 0.9436$, $R^2_{\text{3-picoline}} = 0.9951$, $R^2_{\text{4-picoline}} = 0.9912$, and $R^2_{\text{2,4-lutidine}} = 0.9317$, respectively, are observed.

Table 2 The electric potential for elements of pyridine and its privatives that was adsorbed on the Al–Al surface by CAM-B3LYP/EPR-III, 6–31 + G(d,p) calculation extracted of NQR method

Atom type	Pyridine	Atom type	2-picoline	Atom type	3-PICOLINE	Atom type	4-PICOLINE	Atom type	2,4-LUTIDINE
N1	− 18.1114	N1	− 18.115136	N1	− 18.110144	N1	− 18.112662	N1	− 18.121783
C2	− 14.5086	C2	− 14.516368	C2	− 14.517693	C2	− 14.516211	C2	− 14.52114
C3	− 14.5086	C3	− 14.506846	C3	− 14.519341	C3	− 14.516054	C3	− 14.51142
C4	− 14.5376	C4	− 14.54768	C4	− 14.532927	C4	− 14.547136	C4	− 14.555813
C5	− 14.5275	C5	− 14.537316	C5	− 14.539921	C5	− 14.5262	C5	− 14.531572
C6	− 14.5376	C6	− 14.545873	C6	− 14.543523	C6	− 14.54722	C6	− 14.554003
C7	− 1.13554	C7	− 14.536675	C7	− 14.529742	C7	− 14.527281	C7	− 14.539233
C8	− 1.13556	H8	− 1.123562	H8	− 1.124348	H8	− 1.123384	C8	− 14.530294
H9	− 1.1264	H9	− 1.123551	H9	− 1.123569	H9	− 1.123247	H9	− 1.127589
H10	− 1.12628	H10	− 1.118441	H10	− 1.118189	H10	− 1.122598	H10	− 1.128015
H11	− 1.12641	H11	− 1.123821	H11	− 1.121914	H11	− 1.122607	H11	− 1.128148
		H12	− 1.14265	H12	− 1.134918	H12	− 1.132548	H12	− 1.145187
		H13	− 1.144245	H13	− 1.140255	H13	− 1.138134	H13	− 1.146726
		H14	− 1.14265	H14	− 1.134911	H14	− 1.132548	H14	− 1.145187
								H15	− 1.135508
								H16	− 1.141087
								H17	− 1.135508

In addition, it observed the effect of substitution of aluminum atoms on Al–Al surface with magnesium, gallium, and silicon in aluminum alloys (Al–Mg, Al–Ga, and Al–Si) through resulting electric potential using NQR analysis (Fig. 3). It is obvious that the graph of Al–Al is fluctuated by Mg, Ga, and Si atoms in the related alloys. Fig. 3 remarks the changes of electric potential for nitrogen, carbon, hydrogen, aluminum, magnesium, gallium, and silicon, in Al-X(X = Mg, Ga, Si).

3.3 Theory of Natural Bond Orbitals (NBO)

"NBO" analysis of pyridine and four derivatives of 2-picoline, 3-picoline, 4-picoline, and 2, 4-lutidine has illustrated the character of electronic conjugation between bonds in the inhibitor and aluminum alloys (Table 3 & Fig. 4).

It observed the fluctuation of occupancy of natural bond orbitals for pyridine → Al–Al, pyridine → Al–Mg, pyridine → Al–Ga, pyridine → Al–Si; 2-picoline → Al–Al, 2-picoline → Al–Mg, 2-picoline → Al–Ga, 2-picoline → Al–Si; 3-picoline → Al–Al, 3-picoline → Al–Mg, 3-picoline → Al–Ga, 3-picoline → Al–Si, 4-picoline → Al–Al, 4-picoline → Al–Mg, 4-picoline → Al–Ga, 4-picoline → Al–Si, and 2,4- lutidine → Al–Al, 2,4- lutidine → Al–Mg, 2,4-lutidine → Al–Ga, and 2,4- lutidine → Al–Si accompanying the Langmuir adsorption model by exhibiting the active nitrogen atom in heterocyclic compounds becoming near the nanosurface (Fig. 4).

3.4 Spectroscopy of Infrared (IR)

"IR" calculations were carried out for three aluminum alloys containing Al–Mg, Al–Ga, and Al–Si, and the organic heterocyclic inhibitors including pyridine, 2-picoline, 3-picoline, 4-picoline and 2,4-lutidine adsorbed onto these alloys surface. Therefore, it has modeled the several complexes, including pyridine → Al–Al, pyridine → Al–Mg, pyridine → Al–Ga, pyridine → Al–Si; 2-picoline → Al–Al, 2-picoline → Al–Mg, 2-picoline → Al–Ga, 2-picoline → Al–Si; 3-picoline → Al–Al, 3-picoline → Al–Mg, 3-picoline → Al–Ga, 3-picoline → Al–Si, 4-picoline → Al–Al, 4-picoline → Al–Mg, 4-picoline → Al–Ga, 4-picoline → Al–Si, and 2,4-lutidine → Al–Al, 2,4-lutidine → Al–Mg, 2,4-lutidine → Al–Ga, and 2,4-lutidine → Al–Si. These structures have been computed at CAM-B3LYP level of theory applying 6 − 31 + G (d,p) /EPR-III /LANL2DZ basis sets to obtain the more accurate equilibrium geometrical parameters, physical and thermodynamic properties for each of the determined structure (Table 4).

Based on Fig. 5a–e, the "IR" spectroscopy analysis, it has been resulted that this protective film contains the inhibitor → Al-X (X = Al, Mg, Ga, Si) complexes. The "IR" spectrum for each of these compounds was indicated in the frequency range between 500 cm^{-1} and 3500 cm^{-1} by the strongest peaks about 550 cm^{-1}, 3250 cm^{-1}, 1750 cm^{-1}, 2000 cm^{-1}, 2800 cm^{-1}, for pyridine → Al–Si, 2-picoline → Al–Si, 3-picoline → Al–Si, 4-picoline → Al–Si and 2, 4-lutidine → Al–Si, respectively (Fig. 5a–e).

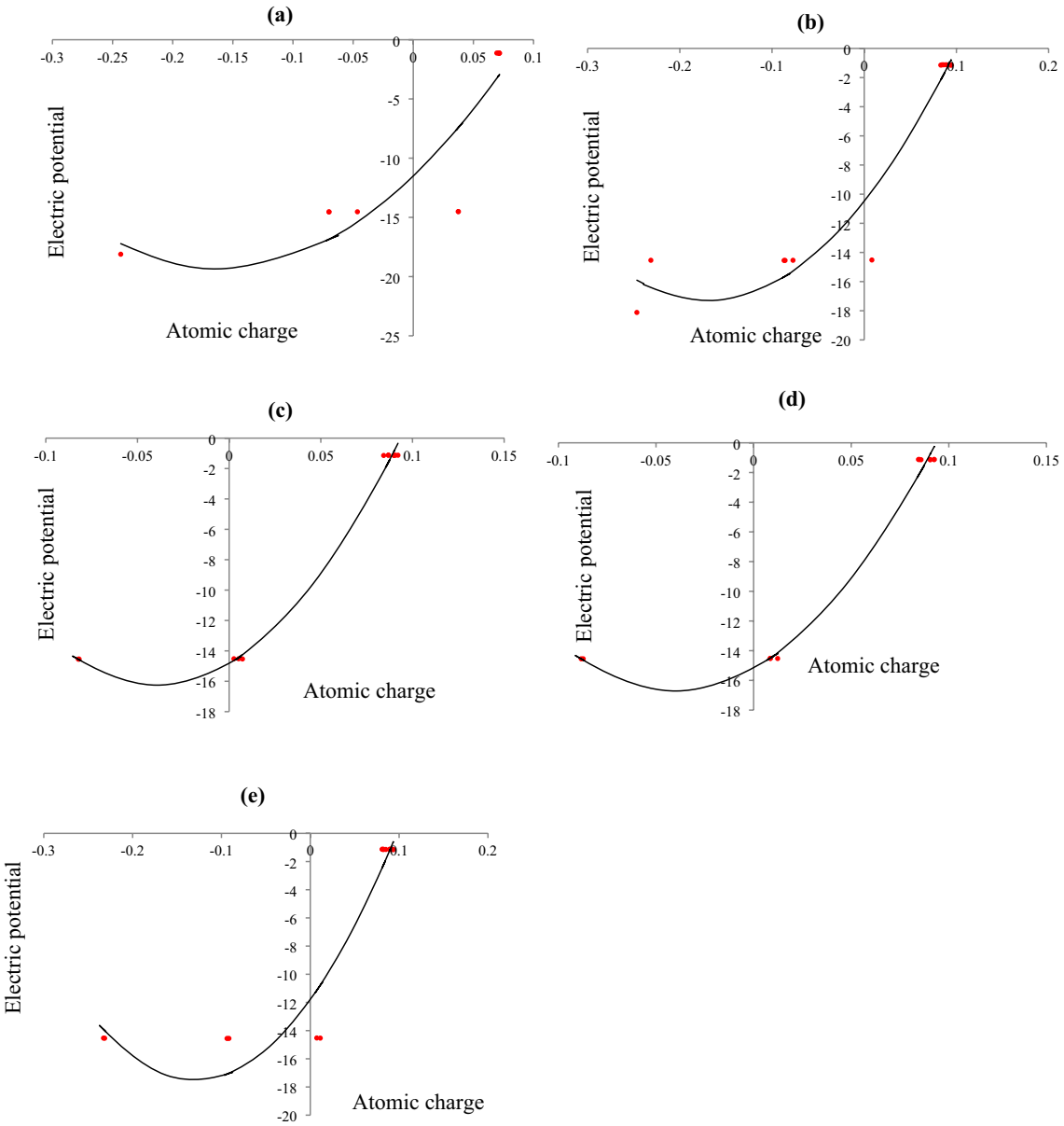

Fig. 2 The electric potential versus atomic charge through NQR calculation for **a** pyridine, **b** 2-picoline, **c** 3-picoline, **d** 4-picoline, and **e** 2,4-lutidine adsorbing on the Al–Al surface using CAM-B3LYP/EPR-III, LANL2DZ,6−31 + G(d,p)

The amounts of ΔG^{o}_{ads} versus dipole moment for pyridine → Al–Al, pyridine → Al–Mg, pyridine → Al–Ga, pyridine → Al–Si; 2-picoline → Al–Al, 2-picoline → Al–Mg, 2-picoline → Al–Ga, 2-picoline → Al–Si; 3-picoline → Al–Al, 3-picoline → Al–Mg, 3-picoline → Al–Ga, 3-picoline → Al–Si, 4-picoline → Al–Al, 4-picoline → Al–Mg, 4-picoline → Al–Ga, 4-picoline → Al–Si, and 2,4-lutidine → Al–Al, 2,4- lutidine → Al–Mg, 2,4-lutidine → Al–Ga, and 2,4-lutidine → Al–Si have been plotted in Fig. 6.

For the adsorption mechanism, ΔG^{o}_{ads} is calculated as follows:

$$\Delta G^{o}_{ads} = \Delta G^{o}_{inh\rightarrow Al-X} - \left(\Delta G^{o}_{inh} + \Delta G^{o}_{Al-X}\right); X = Mg,Ga,Si \quad (5)$$

On the basis of data in Table 4, it is predicted that the adsorption of the inhibitor on the Al alloy surface might be physical and chemical in nature. As shown in Table 4, all the computed ΔG^{o}_{ads} amounts are close, which exhibits the accord of the evaluated data by all methods and the validity of the computations.

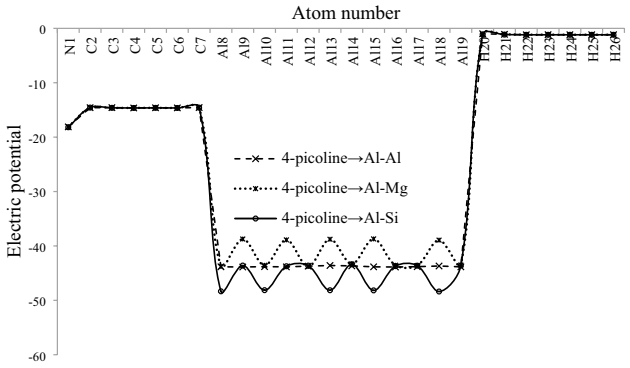

Fig. 3 The changes of the electric potential versus atom number through NQR calculation 4-picoline → Al–Al, 4-picoline → Al–Mg, and 4-picoline → Al–Si complexes accompanying CAM-B3LYP/EPR-III, LANL2DZ,6−31 + G(d,p)

3.5 Frontier Orbitals of HOMO & LUMO

The lowest unoccupied molecular orbital energy "LUMO" and the highest occupied molecular orbital energy "HOMO" were computed for pyridine → Al–Al, pyridine → Al–Mg, pyridine → Al–Ga, pyridine → Al–Si; 2-picoline → Al–Al, 2-picoline → Al–Mg, 2-picoline → Al–Ga, 2-picoline → Al–Si; 3-picoline → Al–Al, 3-picoline → Al–Mg, 3-picoline → Al–Ga, 3-picoline → Al–Si, 4-picoline → Al–Al, 4-picoline → Al–Mg, 4-picoline → Al–Ga, 4-picoline → Al–Si, and 2,4- lutidine → Al–Al, 2,4-lutidine → Al–Mg, 2,4-lutidine → Al–Ga, and 2,4-lutidine → Al–Si through the Langmuir adsorption process using CAM-B3LYP/6−31 + G (2d,p), EPR-III, LANL2DZ (Table 5).

The HOMO, LUMO, and band energy gap (ev) indicated the pictorial explanation of the frontier molecular orbitals, which is an important factor for identifying the molecular characteristics of the high coating for aluminum and its alloys against the metal corrosion phenomenon (Table 5).

In other words, the HOMO shows the capability for giving an electron, while the LUMO as an electron acceptor exhibits the capability for achieving an electron. Therefore, the energy gap ($\Delta E = E_{LUMO} - E_{HOMO}$) indicates the energy difference between frontier HOMO and LUMO orbital introducing the stability for the structure and unravels the chemical activity of the molecule. In this work, energy gap establishes how inhibitors interact with the aluminum and its alloys monolayer surface. Besides, frontier molecular orbitals run an important function in the optical and electrical properties like in UV–VIS spectra [111].

Moreover, for getting more conclusive approving in identifying the compound characteristics of this structure, a series of chemical reactivity parameters consisting of chemical potential (μ), electronegativity (χ), hardness (η), softness (ζ), and electrophilicity index (ψ) has been done (Table 4) [112–115]. The amounts of the parameters in Table 4 have exhibited a good stability of pyridine and its family

Table 3 NBO analysis for the organic heterocyclic inhibitor containing (pyridine, 2-picoline, 3-picoline, 4-picoline, 2,4-lutidine) → Al-*X*(*X* = Al, Mg, Ga, Si) structures

Inhibitor → metal & metal alloy surface	Bond orbital	Occupancy	Hybrids	$R_{N\text{-}Al}$ (Å)
Pyridine → Al–Al	BD (1)N 1-C2	1.95179	0.7476 ($sp^{3.54}$)N + 0.6642 ($sp^{2.77}$)C	1.7674
2-picoline → Al–Al	BD (1) N 1-C3	1.93732	0.7639 ($sp^{3.74}$) N + 0.6453 ($sp^{2.23}$) C	1.8015
3-picoline → Al–Al	BD (1) N1-C2	1.95219	0.7585 ($sp^{2.30}$) N + 0.6517 ($sp^{2.68}$) C	1.7790
4-picoline → Al—Al	BD (1) N1-C2	1.94120	0.7585($sp^{2.43}$) N + 0.6516 ($sp^{2.65}$) C	1.7607
2,4-lutidine → Al–Al	BD (1) N1-C2	1.97218	0.7693 ($sp^{3.11}$) N + 0.6389 ($sp^{2.05}$) C	1.7993
Pyridine → Al–Mg	BD (1) N 1-C3	0.97078	0.7702 ($sp^{3.13}$) N + 0.6378 ($sp^{2.24}$) C	1.7754
2-picoline → Al–Mg	BD (1) N1-C2	0.97336	0.7545 ($sp^{4.85}$) N + 0.6562 ($sp^{2.14}$) C	1.8129
3-picoline → Al–Mg	BD (1) N 1-C3	0.96554	0.7731 ($sp^{4.62}$) N + 0.6343 ($sp^{2.18}$) C	1.7819
4-picoline → Al–Mg	BD (1) N 1-C3	0.97144	0.7621 ($sp^{4.36}$) N + 0.6475 ($sp^{2.29}$) C	1.7732
2,4-lutidine → Al–Mg	BD (1) N 1-C3	0.97544	0.7602 ($sp^{4.06}$) N + 0.6497 ($sp^{2.30}$) C	1.8017
Pyridine → Al–Ga	BD (1) N1-C2	1.96366	0.7511 ($sp^{2.98}$) N + 0.6602 ($sp^{1.98}$) C	1.7632
2-picoline → Al–Ga	BD (1) N 1-C3	1.96826	0.7575 ($sp^{3.24}$) N + 0.6529 ($sp^{2.10}$) C	1.8007
3-picoline → Al–Ga	BD (1) N 1-C3	1.94781	0.7514 ($sp^{3.27}$) N + 0.6599 ($sp^{1.97}$) C	1.7743
4-picoline → Al–Ga	BD (1) N1-C2	1.95603	0.7653 ($sp^{3.03}$) N + 0.6437 ($sp^{2.08}$) C	1.7601
2,4-lutidine → Al–Ga	BD (1) N1-C2	1.96875	0.7544 ($sp^{2.69}$) N + 0.6565 ($sp^{2.08}$) C	1.7965
Pyridine → Al–Si	BD (1) N1-C2	0.98320	0.7563 ($sp^{2.84}$) N + 0.6542 ($sp^{2.07}$) C	1.7723
2-picoline → Al–Si	BD (1) N1-C2	0.98608	0.7470 ($sp^{2.92}$) N + 0.6648 ($sp^{2.08}$) C	1.8113
3-picoline → Al–Si	BD (1) N1-C2	0.97756	0.7507 ($sp^{2.93}$) N + 0.6606 ($sp^{2.06}$) C	1.7805
4-picoline → Al–Si	BD (1) N1-C2	0.97961	0.7449 ($sp^{3.42}$) N + 0.6671 ($sp^{1.96}$) C	1.7726
2,4-lutidine → Al–Si	BD (1) N1-C2	0.98425	0.7580 ($sp^{2.81}$) N + 0.6523 ($sp^{2.10}$) C	1.8012

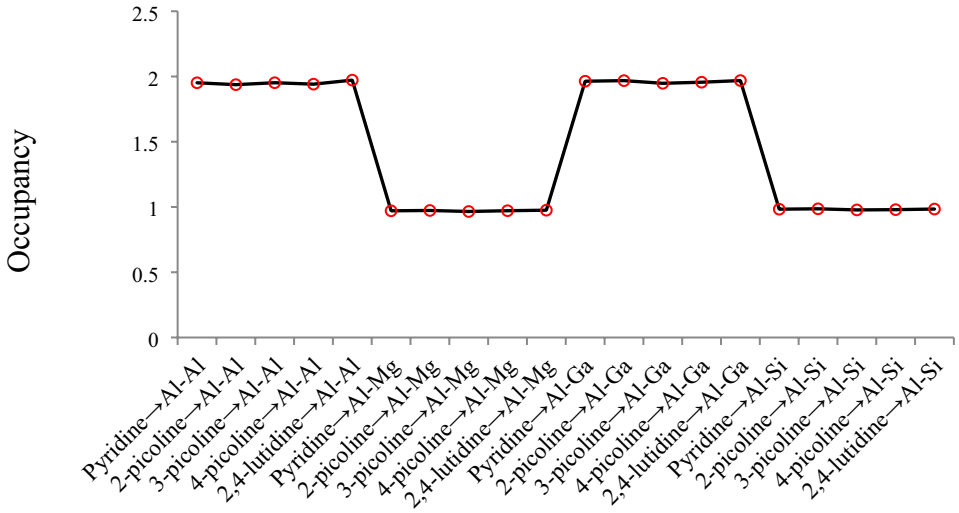

Fig. 4 Diagram of occupancy extracted of NBO method for the organic heterocyclic inhibitors containing (pyridine, 2-picoline, 3-picoline, 4-picoline, 2,4-lutidine) → Al-*X*(*X* = Al, Mg, Ga, Si) structures

Table 4 The Physicochemical properties of adsorption for pyridine, 2-picoline, 3-picoline, 4-picoline, and 2,4-lutidine as corrosion inhibitors on the aluminum and its alloys nanosheet consisting of Al–Mg, Al–Ga, and Al–Si at 300 K

Material	$\Delta E^{o} \times 10^{-4}$ (kcal/mol)	$\Delta H^{o} \times 10^{-4}$ (kcal/mol)	$\Delta G^{o} \times 10^{-4}$ (kcal/mol)	$\Delta G^{o}_{ads} \times 10^{2}$ (kcal/mol)	S^{o} (cal/K.mol)	Dipole moment (Debye)
Al–Al	− 179.9207	− 179.9206	− 179.9229	–	76.078	2.0432
Al–Mg	− 166.2904	− 166.2904	− 166.2926	–	75.228	0.3215
Al–Ga	− 701.4839	− 701.4838	− 701.4861	–	77.743	8.7320
Al–Si	− 193.9035	− 193.9035	− 193.9057	–	75.709	0.9580
Pyridine	− 15.3793	− 15.3792	− 15.3813	–	68.627	2.0338
Pyridine → Al–Al	− 195.2420	− 195.2419	− 195.2444	5.98	82.634	2.4602
Pyridine → Al–Mg	− 181.6098	− 181.6094	− 181.6094	6.45	88.026	2.7271
Pyridine → Al–Ga	− 716.8226	− 716.8226	− 716.8253	4.21	90.206	6.8254
Pyridine → Al–Si	− 209.2550	− 209.2549	− 209.2575	2.95	86.610	5.3876
2-picoline	− 17.8155	− 17.8154	− 17.8176	–	73.692	1.7413
2-picoline → Al–Al	− 197.6544	− 197.6543	− 197.6568	8.37	84.919	2.3156
2-picoline → Al–Mg	− 184.0349	− 184.0348	− 184.0375	7.27	90.184	2.9225
2-picoline → Al–Ga	− 719.2526	− 719.2526	− 719.2554	4.83	94.493	6.7381
2-picoline → Al–Si	− 211.6752	− 211.6752	− 211.6778	4.55	88.037	3.0597
3-picoline	− 17.8154	− 17.8153	− 17.8175	–	73.725	2.2156
3-picoline → Al–Al	− 197.6912	− 197.6912	− 197.6938	4.66	88.341	2.7906
3-picoline → Al–Mg	− 184.0555	− 184.0554	− 184.0580	5.21	87.228	3.7142
3-picoline → Al–Ga	− 719.2376	− 719.2375	− 719.2401	6.35	87.910	5.0212
3-picoline → Al–Si	− 211.6566	− 211.6565	− 211.6591	6.41	85.138	3.5042
4-picoline	− 17.8154	− 17.8154	− 17.8176	–	73.717	2.4672
4-picoline → Al–Al	− 197.6901	− 197.6901	− 197.6927	4.78	89.424	3.1315
4-picoline → Al–Mg	− 184.0535	− 184.0534	− 184.0559	5.43	84.850	2.4644
4-picoline → Al–Ga	− 719.2625	− 719.2624	− 719.2652	3.85	93.203	7.8674
4-picoline → Al–Si	− 211.6786	− 211.6786	− 211.6812	4.21	88.469	4.2218
2,4-lutidine	− 20.2516	− 20.2515	− 20.2539	–	78.728	2.1610
2,4-lutidine → Al–Al	− 200.0561	− 200.0560	− 200.0587	11.81	91.272	2.7164
2,4-lutidine → Al–Mg	− 186.5020	− 186.5020	− 186.5048	4.17	93.257	3.0400
2,4-lutidine → Al–Ga	− 721.6913	− 721.6912	− 721.6941	4.59	95.307	7.0929
2,4-lutidine → Al–Si	− 214.1015	− 214.1014	− 214.1042	5.54	92.919	2.7789

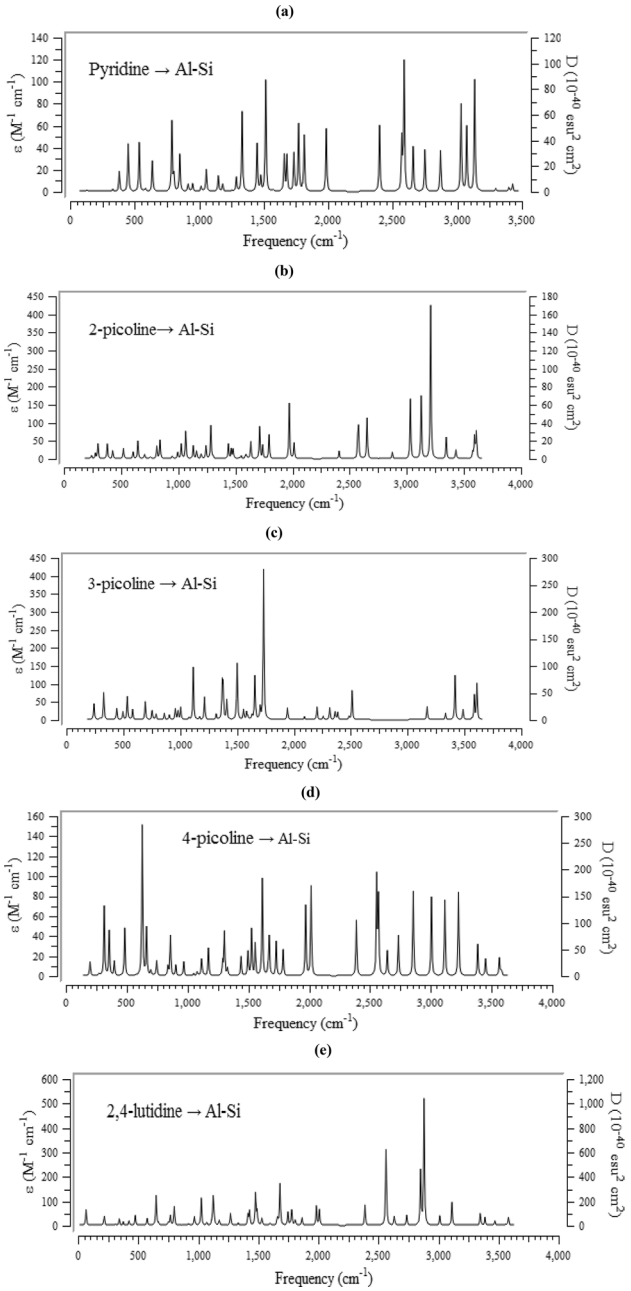

Fig. 5 Diagram of IR spectra for **a** pyridine → Al–Si, **b** 2-picoline → Al–Si, **c** 3-picoline → Al–Si, **d** 4-picoline → Al–Si, and **e** 2, 4-lutidine → Al–Si adsorbed on the Al–Si surface accompanying CAM-B3LYP/EPR-III, LANL2DZ,6−31 + G(d,p) calculations

compounds through Langmuir adsorption on the aluminum and its alloys' monolayer surface.

3.6 UV–VIS spectroscopy

In this investigation, TD-DFT/6 − 31 + G (2d, p), EPR-III, LANL2DZ computations have been also done to identify the low-lying excited states of pyridine, 2-picolone, 3-picoline, 4-picoline, and 2,4-lutidine adsorbed on the Al–Al surface. The results consist of the vertical excitation energies, oscillator strength, and wavelength which have been introduced in Fig. 7a–e.

In fact, based on the computed amounts of UV–VIS spectra for pyridine, 2-picolone, 3-picoline, 4-picoline, and 2,4-lutidine adsorbed on the Al–Al, Al–Mg, Al–Ga, and Al–Si surface, there are maximum adsorption bands between 150 and 240 nm (Fig. 7a–e). Two maximum adsorption bands for pyridine, 2-picoline, 3-picoline, and 4-picoline are at 200 nm and 250 nm (Fig. 7a–c). Besides, it has been observed two maximum adsorption bands for 2,4-lutidine around 170 nm and 210 nm, respectively (Fig. 7e). Moreover, the complexes of Langmuir adsorption containing pyridine → Al–Ga; 2-picoline → Al–Mg; 3-picoline → Al–Ga; 4-picoline → Al–Si; and 2,4-lutidine → Al–Al have been exhibited maximum band wavelengths between 500 and 2500 nm for these compounds (Fig. 7a′–e′). In fact, the sharpest peaks for pyridine → Al–Ga, 1400 nm; 2-picoline → Al–Mg, 1500 nm; 3-picoline → Al–Ga, 1000 nm and 2800 nm; 4-picoline → Al–Si, 2000 nm; and 2,4-lutidine → Al–Al, 1000 nm, respectively (Fig. 7a′–e′).

4 Conclusion

In this research, the adsorption and diffusion of pyridine and its family on the Al alloys surface have been investigated based on Langmuir theory with "ONIOM" method with high, medium, and low levels of EPR-III/6–31 + G(d,p)/LANL2DZ, semi-empirical, and MM2 basis sets, respectively.

The yield of the organic heterocyclic inhibitors as the aluminum alloy coating was illustrated through the thermoelectric characteristics and features of the environmental condition extracted from NMR, NQR, NBO, UV–VIS spectra, HOMO/LUMO frontier orbitals, and other quantum data analysis which have been accomplished on pyridine → Al–Al, pyridine → Al–Mg, pyridine → Al–Ga, pyridine → Al–Si; 2-picoline → Al–Al, 2-picoline → Al–Mg, 2-picoline → Al–Ga, 2-picoline → Al–Si; 3-picoline → Al–Al, 3-picoline → Al–Mg, 3-picoline → Al–Ga, 3-picoline → Al–Si, 4-picoline → Al–Al, 4-picoline → Al–Mg, 4-picoline → Al–Ga, 4-picoline → Al–Si, and 2,4-lutidine → Al–Al, 2,4- lutidine → Al–Mg, 2,4- lutidine → Al–Ga, and 2,4-lutidine → Al–Si.

An elaborate investigation for the mechanism of local minima in the adsorption potential energy landscape

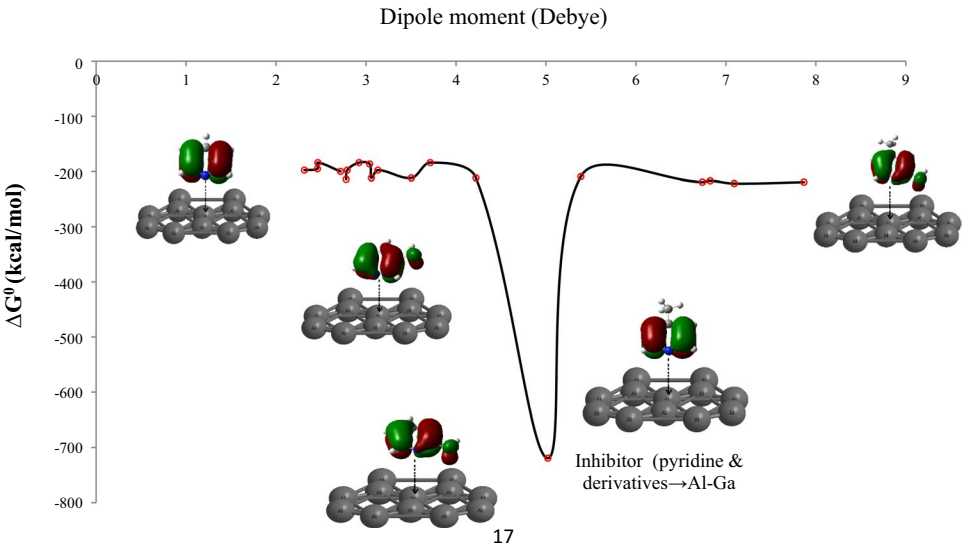

Fig. 6 Gibbs free energy for adsorption of pyridine and its derivatives as corrosion inhibitors on the aluminum alloys nanosheet containing Al–Mg, Al–Ga, and Al–Si versus dipole moment (Debye)

Table 5 The LUMO (a.u.), HOMO (a.u.), band energy gap (ev), and other parameters (ev) for the organic heterocyclic inhibitors containing (pyridine, 2-picoline, 3-picoline, 4-picoline, 2,4-lutidine) → Al-*X*(*X* = Al, Mg, Ga, Si) structures using CAM-B3LYP/6−31 + G (2d,p), EPR-III, LANL2DZ

Inhibitor	HOMO	LUMO	ΔE	μ	χ	η	ζ	ψ
Pyridine → Al–Al	0.0220	0.0542	0.8762	1.0367	− 1.0367	0.4381	1.1413	1.2266
Pyridine → Al–Mg	0.01260	0.0909	2.1306	1.4082	− 1.4082	1.0653	0.4693	0.9307
Pyridine → Al–Ga	− 0.0643	− 0.0047	1.6218	− 0.9388	0.9388	0.8109	0.6166	0.5434
Pyridine → Al–Si	− 0.0118	0.0647	2.0816	0.7197	− 0.7197	1.0408	0.4804	0.2488
2-picoline → Al–Al	0.0386	0.0724	0.9197	1.5102	− 1.5102	0.4598	1.0873	2.4801
2-picoline → Al–Mg	0.0406	0.0960	1.5075	1.8585	− 1.8585	0.7537	0.6633	2.2913
2-picoline → Al–Ga	− 0.0540	− 0.0047	1.3415	− 0.7986	0.7986	0.6707	0.7454	0.4754
2-picoline → Al–Si	0.0026	0.0565	1.4667	0.8041	− 0.8041	0.7333	0.6818	0.4408
3-picoline → Al–Al	0.0392	0.0685	0.7973	1.4653	− 1.4653	0.3986	1.2542	2.6933
3-picoline → Al–Mg	0.0229	0.0825	1.6218	1.4340	− 1.4340	0.8109	0.6166	1.2679
3-picoline → Al–Ga	− 0.0552	− 0.0097	1.2381	− 0.8830	0.8830	0.6190	0.8077	0.6298
3-picoline → Al–Si	− 0.0019	0.0746	2.0816	0.9891	− 0.9891	1.0408	0.4804	0.4700
4-picoline → Al–Al	0.0290	0.0699	1.1129	1.3456	− 1.3456	0.5564	0.8985	1.6271
4-picoline → Al–Mg	0.0283	0.0915	1.7197	1.6299	− 1.6299	0.8598	0.5815	1.5448
4-picoline → Al–Ga	− 0.0495	− 0.0172	0.8789	− 0.9075	0.9075	0.4394	1.1379	0.9371
4-picoline → Al–Si	− 0.0103	0.0468	1.5537	0.4966	− 0.4966	0.7768	0.6436	0.1587
2,4-lutidine → Al–Al	0.0145	0.0636	1.3360	1.0626	− 1.0626	0.6680	0.7485	0.8451
2,4-lutidine → Al–Mg	0.0130	0.0893	2.0762	1.3918	− 1.3918	1.0381	0.4816	0.9330
2,4-lutidine → Al–Ga	− 0.0476	− 0.0138	0.9197	− 0.8353	0.8353	0.4598	1.0874	0.7587
2,4-lutidine → Al–Si	− 0.0025	0.0556	1.5809	0.7224	− 0.7224	0.7904	0.6326	0.3301

$\Delta E = E_{LUMO} - E_{HOMO}$; $\mu = (E_{HOMO} + E_{LUMO})/2$; $\chi = -(E_{HOMO} + E_{LUMO})/2$; $\eta = (E_{LUMO} - E_{HOMO})/2$; $\zeta = 1/(2\eta)$; $\psi = \mu^2/(2\eta)$

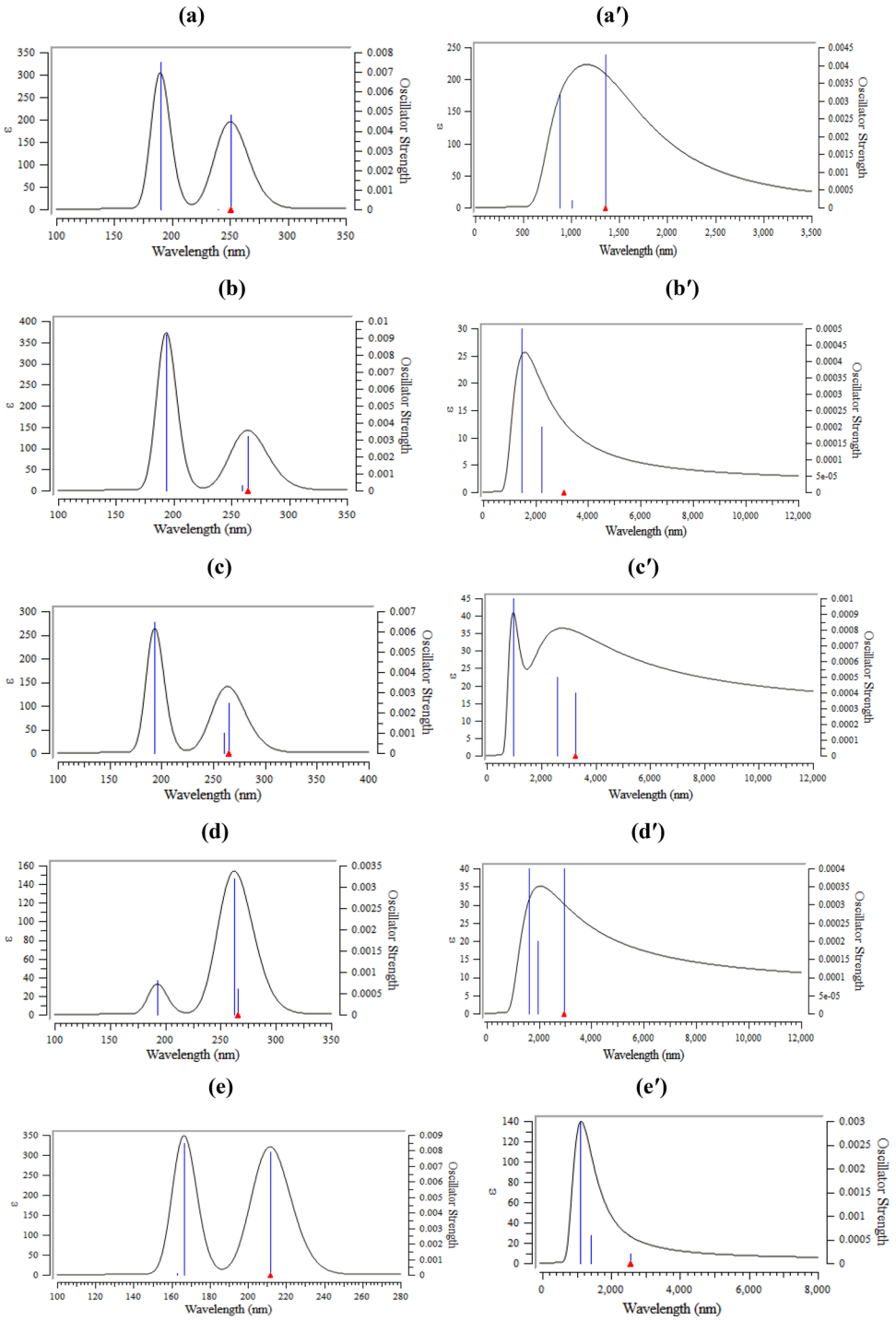

Fig. 7 UV–VIS spectra for organic heterocyclic inhibitors adsorbing on the aluminum and its alloys surface using TD-DFT/6−31 + G (2d,p), EPR-III, LANL2DZ, including **a** pyridine and **a′** pyridine → Al–Ga; **b** 2-picoline and **b′** 2-picoline → Al–Mg; **c** 3-picoline and c′ 3-picoline → Al–Ga; **d** 4-picoline and **d′** 4-picoline → Al–Si; and **e** 2,4-lutidine and **e′** 2,4-lutidine → Al–Al

represents that the intact pyridine, 2-picoline, 3-picoline, 4-picoline, and 2,4-lutidine adsorb with the aromatic ring parallel to the Al alloy nanosheet. In the selected path, the these organic inhibitors remain parallel to the nanosheet while executing small single rotational steps with a "C–C" double bond belonged to above a single aluminum atom in Al–Mg, Al–Ga, and Al–Si.

Author Contributions Conceptualization and idea, FM; Methodology, FM and MM; Software, FM and MM; Validation, FM and MM; Formal analysis, FM and MM; Investigation, FM and MM; Data Curation, FM and MM; Writing of the original draft preparation, FM; Writing, reviewing, and editing of the manuscript, FM and MM; Visualization, FM and MM; Supervision, FM; Resources, MM; Project administration, FM. All authors have read and agreed to the published version of the manuscript.

Funding This research received no external funding.

Data Availability There is no data availability statement.

Declarations

Conflict of interest The authors declare no conflict of interest.

References

1. Ahmad Z, (2006) Principles of Corrosion Engineering and Corrosion Control. Elsevier Science and Technology Books.
2. Monajjemi M, Khaleghian M, Tadayonpour N, Mollaamin F (2010) The effect of different solvents and temperatures on stability of single-walled carbon nanotube: a QM/MD study. Int J Nanosci 09:517–529. https://doi.org/10.1142/S0219581X10007071
3. Yang HM, Qiu ZX, Zhang G (2009) Low Temperature Aluminum Electrolysis. Northeast University Press, Shenyang
4. Lu HM, Qiu ZX (1997) Research progress of low temperature aluminum electrolysis. Light Metals 4:24
5. Monajjemi M, Baie MT, Mollaamin F (2010) Interaction between threonine and cadmium cation in [Cd(Thr) n]2+ (n = 1–3) complexes: density functional calculations. Russ Chem Bull 59:886–889
6. Mollaamin F, Monajjemi M (2015) Harmonic linear combination and normal mode analysis of semiconductor nanotubes vibrations. J Comput Theor Nanosci 12:1030–1039
7. Wasserscheid P, Welton T (2008) Ionic Liquids in Synthesis. Wiley, Hoboken
8. Zhang M, Kamavarum V, Reddy RG (2003) New electrolytes for aluminum production. Ionic liquids JOM 55:54
9. Tian GC, Li J, Hua YX (2009) Application of ionic liquids in metallurgy of nonferrous metals. Chin J Process Eng 9:200
10. Tian GC, Li J, Hua YX (2010) Application of ionic liquids in hydrometallurgy of nonferrous metals. Trans Nonferrous Met Soc China 20:513
11. Kwolek P, Dychtoń K, Kościelniak B, Obłój A, Podborska A, Wojnicki M (2022) Gallic acid as a potential green corrosion inhibitor for aluminum in acidic solution. Metals 12:250
12. Tian GC (2019) Ionic liquids as green electrolytes for Aluminum and Aluminum-alloy production. Mater Res Found 54:249
13. Zhong XW, Xiong T, Lu J, Shi ZN (2014) Advances of electrodeposition and aluminum refining of aluminum and aluminum alloy in ionic liquid electrolytes system. Nonferrous Met Sci Eng 5:44
14. Zheng Y, Wang Q, Zheng YJ, Lv HC (2015) Advances in research and application of aluminum electrolysis in ionic liquid systems. Chin J Process Eng 15:713
15. Fleury V, Kaufman JH, Hibbert DB (1994) Mechanism of a morphology transition in ramified electrochemical growth. Nature 367:435
16. Yue G, Lu X, Zhu Y, Zhang X, Zhang S (2009) Surface morphology, crystal structure and orientation of aluminum coatings electrodeposited on mild steel in ionic liquid. Chem Eng J 147:79
17. Tarantella G (1991) Whitney award lecture: inhibitors—An old remedy for a new challenge. Corrosion 47:410
18. Schmitt G (1984) Application of inhibitors for acid media: report prepared for the European federation of corrosion working party on inhibitors. Corros J 19:165
19. Bockris, J.O'M., Yang, B., (1991)The mechanism of corrosion inhibition of iron in acid solution by acetylenic alcohols. J.Electrochem.Soc 138:2237
20. Growcock FB, Lopp VR (1988) The inhibition of steel corrosion in hydrochloric acid with 3-phenyl-2-propyn-1-ol. Corros Sci 28:397
21. Bartos M, Hackerman N (1992) A Study of Inhibition Action of Propargyl Alcohol during Anodic Dissolution of Iron in Hydrochloric Acid. J Electrochem Soc 139(3):429
22. Zucchi F, Trabanelli G, Brunoro G (1992) The influence of the chromium content on theinhibitive efficiency of some organic compounds. Corros Sci 33(1):135
23. Mollaamin, F., Monajjemi, M. (2023) Transition metal (X = Mn, Fe, Co, Ni, Cu, Zn)-doped graphene as gas sensor for CO2 and NO2 detection: a molecular modeling framework by DFT perspective. J Mol Model 29:119
24. Tadros AB, Abdenaby BA (1988) Inhibition of the acid corrosion of steel by 4-amino-3-hydrazino-5-thio-1,2,4-triazoles. J Electroanal Chem 246:433
25. Mernari B, Elattari H, Traisnel M, Bentiss F, Lagreence M (1998) Inhibiting effects of 3,5-bis(n-pyridyl)-4-amino-1,2,4-triazoles on the corrosion for mild steel in 1 M HCl medium. Corros Sci 40:391
26. Bentiss F, Lagreence M, Traisnel M (1999) The corrosion inhibition of mild steel in acidic media by a new triazole derivative. Corros Sci 41:789
27. Bentiss F, Traisnel M, Lagreence M (2000) The substituted 1,3,4-oxadiazoles: a new class of corrosion inhibitors of mild steel in acidic media. Corros Sci 42:127
28. Hackerman N, Makrides AC (1954) Action of polar organic inhibitors in acid dissolution of metals. Ind Engng Chem 46:523
29. Aramaki K, Hackerman N, (1968)Structure Effects of Many-Membered Polymethyleneimine on Corrosion Inhibition. J Electrochem Soc 115:1007.
30. Barth JV, Brune H, Ertl G, Behm RJ (1990) Scanning tunneling microscopy observations on the reconstructed Au(111) surface: Atomic structure, long-range superstructure, rotational domains, and surface defects. Phys Rev B 42:9307–9318
31. Esken D, Turner S, Lebedev OI, van Tendeloo G, Fischer RA (2010) Au@ ZIFs: stabilization and encapsulation of cavity-size matching gold clusters inside functionalized zeolite imidazolate frameworks. ZIFs Chem Mater 22:6393–6401
32. Mollaamin F, Ilkhani A, Sakhaei N, Bonsakhteh B, Faridchehr A, Tohidi S, Monajjemi M (2015) Thermodynamic and solvent effect on dynamic structures of nano bilayer-cell membrane: hydrogen bonding study. J Comput Theor Nanosci 12:3148–3154
33. Liu B, Smit B (2010) Molecular simulation studies of separation of CO_2/N_2, CO_2/CH_4, and CH_4/N_2 by ZIFs. J Phys Chem C 114:8515–8522
34. Keskin S (2010) Atomistic simulations for adsorption, diffusion, and separation of gas mixtures in zeolite imidazolate frameworks. J Phys Chem C 115:800–807
35. Tran UPN, Le KKA, Phan NTS (2011) Expanding applications of metal- organic frameworks: zeolite imidazolate framework ZIF-8 as an efficient heterogeneous catalyst for the knoevenagel reaction. ACS Catal 1:120–127
36. VandeVondele J, Krack M, Mohamed F, Parrinello M, Chassaing T, Hutter J (2005) Quickstep: fast and accurate density functional calculations using a mixed Gaussian and plane waves approach. Comp Phys Comm 2:103–128
37. Phan A, Doonan CJ, Uribe-Romo FJ, Knobler CB, O'keeffe M, Yaghi OM (2010) Synthesis, structure, and carbon dioxide capture properties of zeolitic imidazolate frameworks. Acc Chem Res 43:58–67

38. Hohenberg P, Kohn W (1964) Inhomogeneous electron gas. Phys Rev B 136:B864–B871
39. Kohn W, Sham LJ (1965) Self-consistent equations including exchange and correlation effects. Phys Rev 140:A1133–A1138
40. Lippert G, Hutter J, Parrinello M (1997) A hybrid Gaussian and plane wave density functional scheme. Mol Phys 92:477–487
41. Hartwigsen C, Goedecker S, Hutter J (1998) Relativistic separable dual-space Gaussian pseudopotentials from H to Rn. Phys Rev B 58:3641–3662
42. Perdew JP, Burke K, Ernzerhof M (1996) Generalized gradient approximation made simple. Phys Rev Lett 77:3865–3868
43. VandeVondele J, Hutter J (2007) Gaussian basis sets for accurate calculations on molecular systems in gas and condensed phases. J Chem Phys. https://doi.org/10.1063/12770708
44. Méndez CM, Gervasi CA, Pozzi G, Ares AE (2023) Corrosion inhibition of aluminum in acidic solution by *Ilex paraguariensis* (Yerba Mate) extract as a green inhibitor. Coatings 13:434
45. Mavrikakis M, Stoltze P, Nørskov JK (2000) Making gold less noble. Catal Lett 64:101–106
46. Mollaamin F, Monajjemi M (2023) Doping of graphene nanostructure with iron, nickel and zinc as selective detector for the toxic gas removal: a density functional theory study. C 9:20. https://doi.org/10.3390/c9010020
47. Whitman LJ, Stroscio JA, Dragoset RA, Celotta RJ (1991) Geometric and electronic properties of Cs structures on III-V (110) surfaces: From 1D and 2D insulators to 3D metals. Phys Rev Lett 66:1338–1341
48. Zadeh MAA, Lari H, Kharghanian L, Balali E, Khadivi R, Yahyaei H, Mollaamin F, Monajjemi M (2015) Density functional theory study and anti-cancer properties of shyshaq plant: in view point of nano biotechnology. J Comput Theor Nanosci 12:4358–4367
49. Yildirim H, Greber T, Kara A (2013) Trends in adsorption characteristics of benzene on transition metal surfaces: role of surface chemistry and van der waals interactions. J Phys Chem C 117:20572–20583
50. Tahan A, Mollaamin F, Monajjemi M (2009) Thermochemistry and NBO analysis of peptide bond: Investigation of basis sets and binding energy. Russ J Phys Chem A 83:587–597
51. Hoefling M, Iori F, Corni S, Gottschalk KE (2010) The conformations of amino acids on a Gold(111) surface. ChemPhysChem 11:1763–1767
52. Bakhshi K, Mollaamin F, Monajjemi M (2011) Exchange and Correlation effect of hydrogen chemisorption on nano V(100) surface: a DFT study by generalized gradient approximation (GGA). J Comput Theor Nanosci 8:763–768. https://doi.org/10.1166/jctn.2011.1750
53. Valencia H, Kohyama M, Tanaka S, Matsumoto H (2009) Ab initio study of EMIM-BF_4 crystal interaction with a Li (100) surface as a model for ionic liquid/Li interfaces in Li-ion batteries. J Chem Phys 131:244705
54. Clarke-Hannaford J, Breedon M, Best AS, Spencer MJ (2019) The interaction of ethylammoniumtetrafluoroborate [$EtNH_3^+$][BF_4^-] ionic liquid on the Li (001) surface, towards understanding early SEI formation on Li metal. Phys Chem Chem Phys 21:10028–10037
55. Zhang QQ (2014) Study on Electrodeposition of Aluminum and Aluminum Alloy in Ionic Liquid. University of Chinese Academy of Sciences, Beijing
56. Cordero B, Gómez V, Platero-Prats AE, Revés M, Echeverría J, Cremades E, Barragán F, Alvarez S (2008) Covalent radii revisited. Dalton Trans 21:2832–2838
57. van der Bondii A (1964) Waals Volumes and Radii. Phys Chem 68:441–451
58. Monajjemi M, Mollaamin F, Gholami MR, Yoosbashizadeh H, Sadrnezhad SK, Passdar H (2003) Quantum chemical parameters of some organic corrosion inhibitors, Pyridine, 2-Picoline 4-Picoline and 2, 4- Lutidine, Adsorption at Aluminum surface in hydrocholoric and nitric acids and comparison between two acidic media. Main Group Met Chem 26:349–362
59. Mollaamin F, Shahriari S, Monajjemi M, Khalaj Z (2022) Nanocluster of Aluminum lattice via organic inhibitors coating: a study of freundlich adsorption. J Cluster Sci. https://doi.org/10.1007/s10876-022-02335-1
60. Mollaamin F, Monajjemi M (2022) Molecular modelling framework of metal-organic clusters for conserving surfaces Langmuir sorption through the TD-DFT/ONIOM approach. Mol Simul. https://doi.org/10.1080/08927022.2022.2159996
61. Winston Revie R (2011) Uhlig's Corrosion Handbook, 3rd edn. Willey, New York
62. Harvey TG (2013) Cerium-based conversion coatings on aluminium alloys: a process review. Corros Eng Sci Technol 48(4):248–269
63. Chaubey N, Savita et al (2016) Corrosion inhibition performance of different bark extracts on aluminium in alkaline solution. J Assoc Arab Univ Basic Appl Sci. https://doi.org/10.1016/j.jaubas.2015.12.003
64. Boughoues Y, Benamira M, Messaadia L, Ribouh N (2020) Adsorption and corrosion inhibition performance of some environmental friendly organic inhibitors for mild steel in HCl solution via experimental and theoretical study. Colloids Surfaces A Physicochem Eng Asp 593:124610. https://doi.org/10.1016/j.colsurfa.2020.124610
65. Özcan M, Solmaz R, Kardaş G, Dehri İ (2008) Adsorption properties of barbiturates as green corrosion inhibitors on mild steel in phosphoric acid. Colloids Surfaces A Physicochem Eng Asp 325:57–63. https://doi.org/10.1016/j.colsurfa.2008.04.031
66. Saranya J, Sowmiya M, Sounthari P, Parameswari K, Chitra S, Senthilkumar K (2016) N-heterocycles as corrosion inhibitors for mild steel in acid medium. J Mol Liq 216:42–52. https://doi.org/10.1016/j.molliq.2015.12.096
67. Guimarães TAS et al (2020) Nitrogenated derivatives of furfural as green corrosion inhibitors for mild steel in HCl solution. J Mater Res Technol 9:7104–7122. https://doi.org/10.1016/j.jmrt.2020.05.019
68. Özcan M (2008) Interfacial behavior of cysteine between mild steel and sulfuric acid as corrosion inhibitor. Acta Physico-Chimica Sin 24:1387–1392. https://doi.org/10.1016/S1872-1508(08)60059-5
69. Singh A et al (2015) Porphyrins as corrosion inhibitors for N80 steel in 3.5% NaCl solution: electrochemical, quantum chemical, QSAR and Monte Carlo simulations studies. Molecules 20:15122–15146. https://doi.org/10.3390/molecules200815122
70. Ali SA, Mazumder MAJ, Nazal MK, Al-Muallem HA (2020) Assembly of succinic acid and isoxazolidine motifs in a single entity to mitigate CO_2 corrosion of mild steel in saline media. Arab J Chem 13:242–257. https://doi.org/10.1016/j.arabjc.2017.04.005
71. Amar H, Benzakour J, Derja A, Villemin D, Moreau B (2003) A corrosion inhibition study of iron by phosphonic acids in sodium chloride solution. J Electroanal Chem 558:131–139. https://doi.org/10.1016/S0022-0728(03)00388-7
72. El-Sayed MS (2011) Corrosion and corrosion inhibition of aluminum in Arabian Gulf seawater and sodium chloride solutions by 3-amino-5- mercapto-1,2,4-triazole. Int J Electrochem Sci 6:1479–1492
73. Sherif ES (2014) A comparative study on the electrochemical corrosion behavior of iron and X-65 steel in 4.0 wt % sodium chloride solution after different exposure intervals. Molecules 19:9962–9974. https://doi.org/10.3390/molecules19079962

74. Yang D, Zhang M, Zheng J, Castaneda H (2015) Corrosion inhibition of mild steel by an imidazolium ionic liquid compound: the effect of pH and surface pre-corrosion. RSC Adv 5:95160–95170. https://doi.org/10.1039/C5RA14556B
75. Amberchan G et al (2022) Aluminum nanoparticles from a Ga–Al composite for water splitting and hydrogen generation. ACS Appl Nano Mater. https://doi.org/10.1021/acsanm.1c04331
76. Finšgar M, Milošev I (2010) Inhibition of copper corrosion by 1,2,3-benzotriazole: a review. Corros Sci 52(9):2737–2749. https://doi.org/10.1016/j.corsci.2010.05.002
77. Shen AY, Wu SN, Chiu CT (1999) Synthesis and cytotoxicity evaluation of some 8-hydroxyquinoline derivatives. J Pharm Pharmacol 51(5):543–548. https://doi.org/10.1211/0022357991772826
78. CABASSI PAJ et al (1983) The improved flotation of gold from the residues of Orange Free State ores (PDF). J S Afr Inst Min Metall 83(11):270–276
79. Lasagni F, Lasagni A, Marks E, Holzapfel C, Mücklich F, Degischer H (2007) Three-dimensional characterization of 'as-cast' and solution-treated $AlSi_{12}$(Sr) alloys by high-resolution FIB tomography. Acta Mater 55:3875–3882
80. Requena G, Garcés G, Rodríguez M, Pirling T, Cloetens P (2009) 3D architecture and load partition in eutectic Al–Si alloys. Adv Eng Mater 11:1007–1014
81. Asghar Z, Requena G, Kubel F (2010) The role of Ni and Fe aluminides on the elevated temperature strength of an $AlSi_{12}$ alloy. Mater Sci Eng, A 527:5691–5698
82. Stadler F, Antrekowitsch H, Fragner W, Kaufmann H, Uggowitzer P (2012) Effect of main alloying elements on strength of Al–Si foundry alloys at elevated temperatures. Int J Cast Met Res 25:215–224
83. Monajjemi M, Honaparvar B, Khalili Hadad B, Ilkhani A, Mollaamin F (2010) Thermo-chemical investigation and NBO analysis of some anxileotic as nano- drugs. Afr J Pharm Pharmacol 4:521–529
84. Karplus M, Karplus M (2014) Development of multiscale models for complex chemical systems: from H+ H2 to biomolecules (Nobel lecture). Angew Chem Int Ed 38:9992
85. Senn HM, Thiel W (2009) QM/MM methods for biomolecular systems. Angew Chem Int Ed 48:1198
86. Svensson M, Humbel S, Froese RDJ, Matsubara T, Sieber S, Morokuma K (1996) ONIOM: A Multilayered Integrated MO + MM Method for Geometry Optimizations and Single Point Energy Predictions A Test for Diels−Alder Reactions and Pt(P(t-Bu)3)2 + H2 Oxidative Addition. J Phys Chem 100(50):19357–19363. https://doi.org/10.1021/jp962071j
87. Ming-Dao L, Lu-An Y, Qing-Yu W, Xiao-CiY, Xiao-Dong Y, Jin-Yun Z (1996) A STUDY ON CORRELATION BETWEEN ELECTRONIC STRUCTURE AND INHIBITION PROPERTIES OF FIVE-MEMBERED DINITROGEN HETEROCYCLIC COMPOUNDS. J Chin Soc Corros Prot 16:3195
88. Sokkar P, Boulanger E, Thiel W, Sanchez-Garcia E (2015) Hybrid quantum mechanics/molecular mechanics/coarse grained modeling: a triple-resolution approach for biomolecular systems. J Chem Theory Comput. https://doi.org/10.1021/ct500956u
89. Brandt F, Jacob CR (2022) Systematic QM region construction in QM/MM Calculations based on uncertainty quantification. J Chem Theory Comput 18(4):2584–2596. https://doi.org/10.1021/acs.jctc.1c01093
90. Mollaamin F, Monajjemi M, Salemi S, Baei MT (2011) A dielectric effect on normal mode analysis and symmetry of BNNT nanotube. Fuller Nanotub Carbon Nanostructures 19:182–196. https://doi.org/10.1080/15363831003782932
91. Chermette H (1998) Density functional theory. Coord Chem Rev 180:699
92. Chermette H (1999) Chemical reactivity indexes in density functional theory. J Comput Chem 20:129
93. Kohn W, Becke AD, Parr RG (1996) Density functional theory of electronic structure. J Phys Chem 100:12974–12980. https://doi.org/10.1021/jp9606691
94. Ladeira ACQ, Ciminelli VST, Duarte HA, Alves MCM, Ramos AY (2001) Mechanism of anion retention from EXAFS and density functional calculations: arsenic (V) adsorbed on gibbsite. Geochim Cosmochim Acta 65:1211
95. Sousa SF, Fernandes PA, Ramos MJ (2007) General performance of density functionals. J Phys Chem A 111:10439
96. Koch W, Holthausen MC (2001) A Chemist's Guide to Density Functional Theory. Wiley-VCH, New York
97. Becke AD (1993) Density-functional thermochemistry. III. The role of exact exchange. J Chem Phys 98:5648–5652
98. Lee C, Yang W, Parr RG (1988) Development of the Colle-Salvetti correlation-energy formula into a functional of the electron density. Phys Rev B 37:785–789
99. Stephens PJ, Devlin FJ, Chabalowski CF, Frisch MJ (1994) Ab Initio Calculation of Vibrational Absorption and Circular Dichroism Spectra Using Density Functional Force Fields. J Phys Chem 98(45):11623–11627. https://doi.org/10.1021/j100096a001
100. Cramer CJ (2004) Essentials of Computational Chemistry: Theories and Models, 2nd Edition Wiley. Wiley.com. Accessed -06-2021.
101. Vosko SH, Wilk L, Nusair M (1980) Accurate spin-dependent electron liquid correlation energies for local spin density calculations: a critical analysis. Can J Phys 58(8):1200–1211. https://doi.org/10.1139/p80-159
102. Frisch MJ et al. (2016) Gaussian 16, Revision C.01, Gaussian Inc., Wallingford.
103. GaussView, Version 6.06.16, Dennington, Roy; Keith, Todd A, Millam John M, Semichem Inc., Shawnee Mission, KS, 2016.
104. Mollaamin F (2014) Features of parametric point nuclear magnetic resonance of metals implantation on boron nitride nanotube by density functional theory/electron paramagnetic resonance. J Comput Theor Nanosci 11(11):2393–2398
105. Fry RA, Kwon KD, Komarneni S, Kubicki JD, Mueller KT (2006) Solid-state NMR and computational chemistry study of mononucleotides adsorbed to alumina. Langmuir 22:9281–9286
106. Smith JAS (1971) Nuclear quadrupole resonance spectroscopy. J Chem Educ 48:39–41
107. Appendix K: Nuclear quadrupole resonance, by Allen N, Garroway, Naval Research Laboratory. In Jacqueline MacDonald JR. Lockwood: Alternatives for Landmine Detection. Report MR-1608, Rand Corporation, 2003.
108. Poleshchuck OKh, Kalinna EL, Latosinska JN, Koput J (2001) Anisotropic polarizabilities and hyperpolarizabilities of second-period cations. J Mol Struct (THEOCHEM) 547:233–243
109. Young HA, Freedman RD (2012) Sears and Zemansky's University Physics with Modern Physics, 13th edn. Addison-Wesley, Boston, p 754
110. Aihara J (1999) Reduced HOMO−LUMO gap as an index of kinetic stability for Polycyclic aromatic hydrocarbons. J Phys Chem A 103(37):7487–7495. https://doi.org/10.1021/jp990092i
111. Parr RG, Pearson RG (1983) (1983) Absolute hardness: companion parameter to absolute electronegativity. J Am Chem Soc 105:7512–7516. https://doi.org/10.1021/ja00364a005
112. Politzer P, Abu-Awwad F (1998) A comparative analysis of Hartree–Fock and Kohn–Sham orbital energies. Theor Chem Acc 99:83–87. https://doi.org/10.1007/s002140050307
113. Levitt M (2014) Birth and future of multiscale modeling for macromolecular systems (Nobel Lecture). Angew Chem Int Ed 38:10006

114. Warshel A (2014) Multiscale modeling of biological functions: from enzymes to molecular machines (Nobel Lecture). Angew Chem Int Ed 38:10020
115. Senn HM, Thiel W (2007) In Atomistic Approaches in Modern Biology: In: Reiher M (Ed.), Quantum Chemistry to Molecular Simulations, Vol. 268, Springer, New York.